
Photonic Components for Analog Fiber Links

Alejandro García Juárez, Ignacio Enrique Zaldívar Huerta,
Jorge Rodríguez Asomoza and María del Rocío Gómez Colín

Additional information is available at the end of the chapter

<http://dx.doi.org/10.5772/48416>

1. Introduction

Currently, several companies are involved in the transport of radiofrequency (RF) or microwave signals radio over fiber links (RoF). RoF links are considered a promising technique in providing broadband wireless access services in the emerging optical-wireless networks. The modulation scheme which decides the way to generate the optical millimeter-wave signal is a key technique in this optical-wireless access network architecture [1–3]. The simplest RoF system consists of a Central Site (CS) and a Remote Site (RS) connected by an optical fiber link or network. The frequencies of the radio signals distributed by RoF systems span a wide range (usually in the GHz region) and the applications for such systems range from in-building distribution of wireless signals (for example in shopping malls and tunnels), wireline interconnections between base stations and microcellular antennas, antenna remoting for various commercial (wing-tip antennas in aircraft) and military radar systems and broadcasting of cable television signals in both hybrid fiber coax (HFC) and triplexer based fiber-to-the-home (FTTH) systems [4]. On the other hand a traditional RF photonic link operating at 1550 nm consists of a directly modulated DFB laser diode, a length of fiber optic as transmission medium, and a photo-detector (PD) [5]. The fiber chromatic dispersion intrinsically occurring in standard 1550 nm single-mode fibers (SMFs) is one of the main drawbacks that limit the transmission distance and operation bandwidth of such RF fiber-optic systems. However if low dispersion fiber is used in conjunction with an appropriate choice of the laser operating parameters the system becomes quasi linear [6]. DFB lasers are the proper light sources for these applications because of their single longitudinal mode, with side-mode suppression ratio (SMSR) in the order of 40 dB, and stable operation with a narrow spectral width. However, the characteristic relaxation oscillations peak in the laser intensity which produce sidebands on both sides of the main laser line, impose a limiting factor on the proximity of two channels in a communication system. Besides these characteristics, limit the high frequency response of semiconductor lasers and the sensitivity in low frequency applications. In order for an optical analog

transmission of GHz-range signal to be successful in RoF systems, it is necessary to have a good DFB laser without their inherently serious problem of the modulation distortion caused by several factors: spatial-hole burning (SHB), leakage current, nonlinear interaction of carriers and photons, gain compression, nonlinear I-V characteristics in a p-n heterojunction, and power dependent absorption and including relaxation oscillation frequencies. However, recently the authors have demonstrated in reference [7] that when a DFB laser biased in the low laser threshold current region, relaxation oscillation frequencies in the laser intensity appear. These frequencies were seen as sidebands on both sides of the main laser line when the optical spectrum was analyzed with a spectrum analyzer. This result allowed the generation of microwave signals on C band using direct detection method. In addition with the proposed experimental setup in [7], the authors also demonstrate an analog NTSC TV signal transmitted and satisfactorily received in a short distance wireline communication system by using relaxation oscillation frequency as an information carrier. The proposed microwave photonic link architecture used to transmit simultaneously a TV signal at 4 and 5 GHz and over 30 km of standard optical fiber is shown in Figure 1.

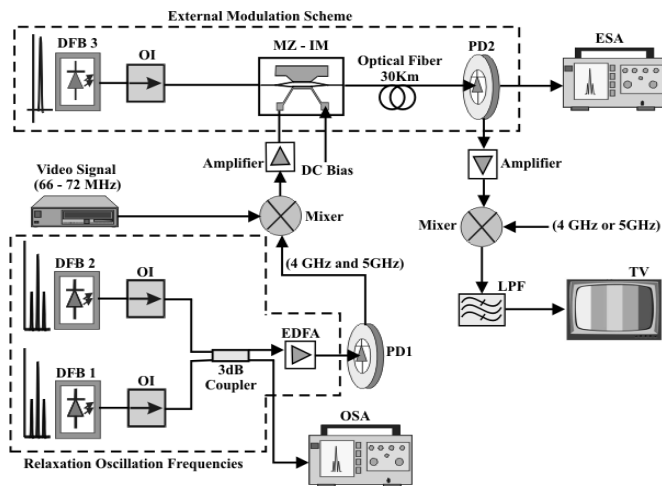


Figure 1. Experimental setup for transmitting a TV signal by using relaxation oscillation frequency as information carrier.

The procedure proposed here starts with the use of two DFB laser diodes emitting at 1550 nm and operating in the low laser threshold current region. When the generated emissions in both lasers are detected by a fast photo-detector using direct detection method, two relaxation oscillation frequencies are obtained. These frequencies acting as information carriers are mixed with TV signals. The signal obtained in the output of the mixer is printed on an optical carrier as an intensity modulation using a MZ-IM. The intensity-modulated optical carrier is then transmitted over 30 km of optical fiber. At the end of the link, a photodiode is used to convert the intensity modulation back to the relaxation oscillation frequencies mixed with TV signals. After that, TV signals are recovered satisfactorily.

In this chapter we start with a brief introduction of microwave photonics. In this first section we describe some schemes for photonic generation of microwave signals with applications in radio-over-fiber systems. After that, in the second section, a detailed theoretical description of the relaxation oscillation frequency in DFB lasers is presented. Moreover, the term photodetection is commonly used here, and we take advantage to introduce the operation principle of direct detection method. In this same section we describe a microwave photonic link by using external modulation. Next, we briefly discuss some passive components suitable for microwave photonics, the main one being optical fiber, but also many of the microwave photonic systems reported in the literature using standard single-mode fiber and associated components such as optical isolators, polarization rotator, polarization control, and optical couplers. In order to show a potential application in the field of communication systems of relaxation oscillation frequencies, it is necessary to report in the last section of this chapter the simultaneous multiplexed transmission of an analog TV signal of 67.25 MHz (TV channel 4) over a photonic link of 30 Km of optical fiber by using two microwave signals at 4 and 5 GHz of our microwave photonic link architecture, giving a signal to noise ratio (SNR) performance of an analog photonic link. Finally our conclusion to this chapter is provided.

2. Microwave photonics

Microwave photonics is an interdisciplinary area that studies the interaction between microwave and optical signals, for applications such as broadband wireless access networks, sensor networks, radar, satellite communications, instrumentation, and warfare systems. In the past few years, there has been an increase effort in researching new microwave photonics techniques for different applications. The major functions of microwave photonic systems include photonic generation, processing, control and distribution of microwave and millimeter-wave (mm-wave) signals. Many research findings have been reported in the last few years. In general, the topics covered by microwave photonics include photonic generation of microwave and mm-wave signals, photonic processing of microwave and mm-wave signals, optically controlled phased array antennas, radio-over-fiber systems, and photonic analog-to-digital conversion. In this section we will emphasize the study of schemes for photonic generation of microwave signals with applications to radio-over-fiber systems.

2.1. Photonic generation of microwave signals

Research into the generation of microwave signals using photonic techniques for various applications such as fiber-radio wireless access networks [8] and phase array antennas [9] has been increasing recently. Techniques which have been proposed and demonstrated include harmonic generation using a MZ-IM [10], heterodyne mixing of two continuous-wave (CW) lasers [11] and resonant enhancement in a monolithic mode-locked laser [12]. Among all these previously reported methods, a favored technique is to use optical heterodyning between two lasing wavelengths whose frequencies are separated by the

desired microwave frequency. Optical heterodyning also has the advantage over other generation techniques of generating high RF power, though optical sources with narrow linewidth or feedback loops are required during operation [13]. The following section includes descriptions of the most common techniques to generate microwave signals using the optical heterodyning method, including optical injection locking (OIL) of laser diodes [14], external modulation technique [15], dual-mode semiconductor laser sources [16] as well as using the optical phase locked loop (OPLL) configuration [17].

2.1.1. Optical heterodyning

The basic principle for generating microwave carriers based on the optical heterodyne technique represents a physical process called optical beating or frequency beating. A PD acting as an optical mixer allow us to obtain a photo-current, which results from the difference between two optical sources emitting at frequencies ω_1 and ω_2 , where $|\omega_1 - \omega_2| \ll \omega_1, \omega_2$. This process is possible when both optical fields are overlapped with common polarization, illuminating a PD of responsivity R ; the resulting photo-current is given by [18].

$$i = R \left[P_1 + P_2 + 2\sqrt{P_1 P_2} \cos((\omega_1 - \omega_2)t + (\phi_1 - \phi_2)) \right] \quad (1)$$

where P_1 and P_2 are the powers and correspond to DC terms, ϕ_1 and ϕ_2 are the phases of the two sources incident on the PD. The term $2\sqrt{P_1 P_2} \cos((\omega_1 - \omega_2)t + (\phi_1 - \phi_2))$, usually called intermediate frequency (IF), represents the microwave carrier generated. Figure 2 shows the experimental setup used for generating microwave signals.

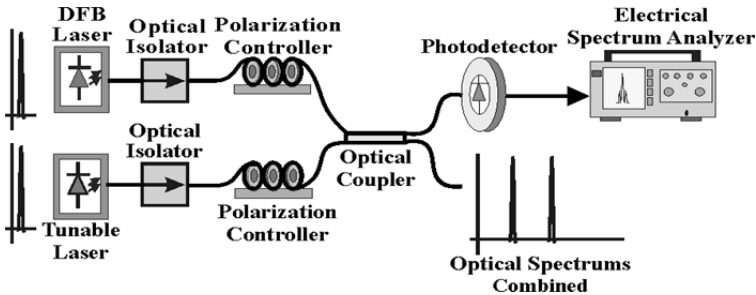


Figure 2. Optical heterodyning for generating microwave signals.

In this experiment two laser diodes emitting at different wavelengths are used. One of them is tunable and can be tuned over the C band with a channel spacing of 25 GHz, and the other is a fiber coupled DFB laser source with a central wavelength at 1550 nm. For the generation of the microwave signals, the outputs of both lasers are coupled to optical isolators to avoid a feedback into the lasers and consequential instabilities to the system. A pair of polarization controllers is used to minimize the angle between the polarization directions of both optical sources. Thus, the polarization of the light issued from each optical

source is matched and therefore, there is no degradation of the power levels in the microwave signals generated in the PD. The output of each controller is launched to a 3 dB coupler to combine both optical spectrums. After that, an optical output signal is received by a fast PD. The resulting photo-current from the PD corresponds to the microwave beat signal which is analyzed with an Electrical Spectrum Analyzer (ESA). The other optical output resulting from an optical coupler is applied to an Optical Spectrum Analyzer (OSA) for monitoring the wavelength of the two beams. DFB laser sources provide the ability to control not only the output optical power of the fiber coupled laser diode, but also the precise the temperature at which the laser is operating. Both controls can be used to tune the fiber coupled laser diode to an optimum operating point, providing a stable output. In this way, we can observe that the wavelength of the DFB laser is shifting by varying its temperature with a scale of 1°C. Consequently, the beat signal frequency is continuously tuned in the bandwidth of the fast PD. Figure 3 illustrates the spectrums of three microwave signals generated with optical heterodyne technique. The generated signals are located at 2.4, 4.9 and 9.5 GHz when the temperature of the DFB laser was tuned at different values of temperatures. The frequency difference from both lasers can be expressed by [19]

$$\Delta f = \frac{c}{\lambda_1} - \frac{c}{\lambda_2} = \frac{c(\lambda_2 - \lambda_1)}{\lambda_1 \lambda_2} \approx \frac{c}{\lambda^2} |\Delta \lambda|^2 \quad (2)$$

where λ_1 and λ_2 are the wavelengths of the two beams, respectively, and $\Delta \lambda$ is the difference between the two wavelengths.

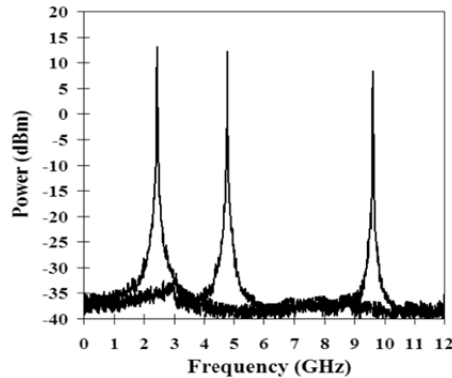


Figure 3. Microwave spectrums continuously tuned from 0 to 10 GHz.

Advantages

Using optical heterodyning, very high frequencies can be generated, limited only by the bandwidth of the photo-detector [20]. Furthermore, heterodyning yields high-detected power (higher link gain) and higher carrier-to-noise ration (CNR). This is so because all the optical powers of the two optical fields contribute to the power of the generated microwave signal.

Disadvantages

Beating two optical waves from two free-running laser diodes would lead to a microwave or mm-wave signal with high phase noise since the phases of the two optical waves are not correlated. They would also be transferred to the generated microwave or mm-wave signal as shown in Eq. (1). Therefore, the generated RF signal is very sensitive to phase noise. Since semiconductor lasers are prone to phase noise, extra measures to minimize the noise have to be taken. Techniques used to reduce phase noise sensitivity, OIL and OPLL, are discussed below.

2.1.2. Optical Injection Locking (OIL)

To generate a high-quality microwave or mm-wave signal, the phase terms of the two optical waves used for heterodyning must be highly correlated. The phase coherence of two laser diodes can be realized by using optical injection locking [21].

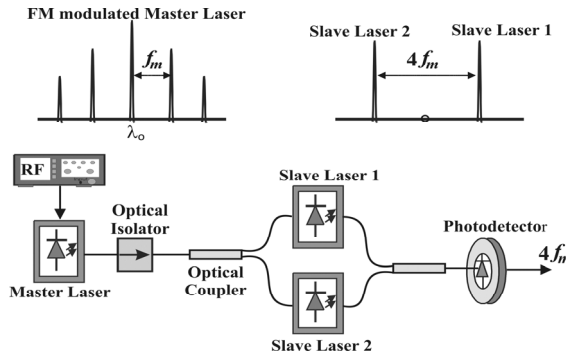


Figure 4. Optical Injection Locking.

Figure 4 shows an optical injection locking system that consists of one master laser and two slave lasers. As can be seen, RF reference is applied to the master laser. Due to frequency modulation (FM) at the master laser, an optical carrier and different orders of optical sidebands are generated at the output of the master laser. The signal at the output of the master laser is then injected into the two slave lasers. The two slave lasers are selected such that their free-running wavelengths are close to two sidebands, that is to say, the +2nd-order and -2nd-order sidebands in Figure 4. Therefore, the wavelengths of the two slave lasers are locked to the +2nd-order and -2nd-order sidebands, optical injection locking is thus achieved [21]. Since the two wavelengths from the two slave lasers are phase correlated, the beating of the two wavelengths at a PD would generate a beat note with low phase noise. In addition, depending on the design, the frequency of the beat note is equal to an integer multiple of the frequency of the RF reference applied to the master laser.

Advantages

One advantage of using OIL is that cheaper broad-linewidth lasers can still be used to generate stable narrow electrical linewidth signals. Secondly, OIL exhibits good phase

noise suppression. Thirdly, because the slave laser locks on to a sub-harmonic of its resonance frequency, low frequency reference signals are used. OIL is simpler and easier to achieve.

Disadvantages

The major disadvantage of OIL is that it has a small frequency detuning range. Optimum phase noise suppression occurs only at one point of slave laser detuning relative to the free-running frequency.

2.1.3. Optical Phase Locked-Loops (OPLL)

Another approach to achieving phase coherence between two optical waves is to use an OPLL, in which the phase of one laser is actively locked to that of a second laser by an OPLL, as shown in Figure 5. This technique has been explored extensively in the past few years [22-24]. To achieve effective phase locking, the two lasers should be selected to have narrow linewidths and therefore have phase fluctuations only at low frequencies, which significantly eases the requirement for a very short feedback loop.

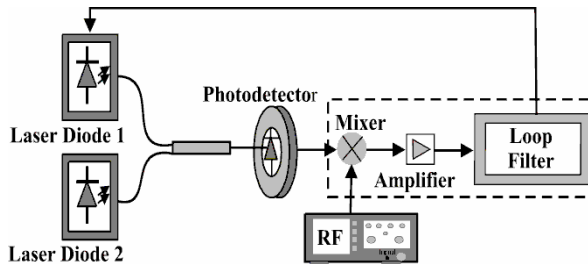


Figure 5. Schematic of an Optical Phase-Locked Loop.

As shown in Figure 5, a beat note is generated at the output of the photo-detector. The phase of the beat note is compared with that of an RF reference from a microwave generator at a mixer followed by a low-pass loop filter. The module in the dotted box is an electrical phase detector, with the output voltage being proportional to the phase difference between the beat note and the RF reference, which is an error voltage that is fed back to control the phase of one of the laser sources by changing the laser cavity length or the injection current. With a proper feedback loop gain and response time, the relative phase fluctuations between the two lasers are significantly reduced and the phase of the beat note is locked to the RF reference.

Advantages

Because OPLL techniques track small phase variations they are capable of producing high quality RF signals with narrow linewidth. OPLLs also have good temperature tracking capabilities. In addition, OPLLs exhibit a wide locking range.

Disadvantages

The major drawback of OPLLs is that they require far more complex laser structures such as 3-contact DFBs. This requirement is a direct consequence of the fact that to track the frequency perturbations of the master laser, the tuning rate of the slave laser must be sufficiently high. This also implies that sufficient feedback bandwidth must be available. The required feedback bandwidth is determined by the summed laser linewidth, the requirements for loop stability, and phase noise requirements placed on the optical microwave signal by the system in which the OPLL is to be applied. A wide feedback bandwidth is necessary if semiconductor lasers are used, because they have a large amount of phase noise. In order to achieve the wide feedback bandwidth, the loop-propagation delay must be small.

2.1.4. Microwave generation based on external modulation

In addition to the techniques using optical injection locking and OPLL, high-quality microwave signals can also be generated based on external modulation [25–27]. A method to generate a mm-wave signal using an external optical modulation technique was first proposed in 1992 [25]. A frequency-doubled electrical signal was optically generated by biasing the MZ-IM to suppress the even-order optical sidebands ($2f$ method). A 36 GHz mm-wave signal was generated when the MZ-IM was driven by an 18 GHz microwave signal. Such a system was employed for a remote delivery of video services [26]. In 1994, another method was proposed to generate a frequency-quadrupled electrical signal ($4f$ method). Instead of biasing the MZ-IM to suppress the even-order optical sidebands, the method in [10] was based on the quadratic response of an optical intensity modulator. The optical carrier and the first and third-order optical sidebands were suppressed by adjusting the drive signal level. A 60 GHz millimeter-wave signal was generated when a 15 GHz drive signal was applied to the MZ-IM.

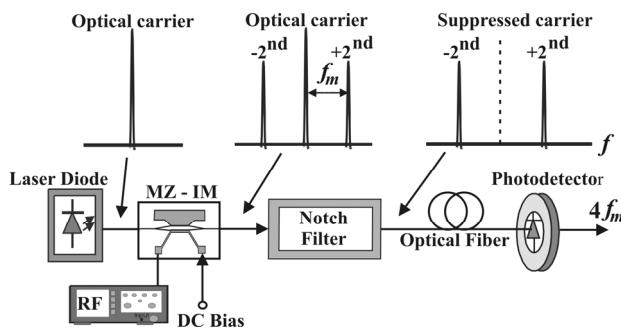


Figure 6. Microwave signal generation based on external modulation.

Figure 6 shows a system to generate a continuously tunable mm-wave signal based on external modulation using a MZ-IM and a wavelength-fixed optical filter [28]. The significance of the technique is that no tunable optical filter is required, which significantly

simplifies the system implementation. As can be seen from Figure 6, the system consists of a MZ-IM that is biased at the maximum transmission point of the transfer function to suppress the odd-order optical sidebands. A fiber Bragg grating (FBG) serving as a wavelength-fixed notch filter is then used to filter out the optical carrier. A stable, low-phase noise mm-wave signal that has four times the frequency of the RF drive signal is generated at the output of the PD.

Advantages of the $2f$ and $4f$ methods

Both the $2f$ and $4f$ methods rely on optical heterodyning. Therefore, they are capable of generating high frequency mm-waves. Since the same laser generates both optical fields, the phase noise is highly correlated resulting in very narrow linewidth mm-waves. In fact, the performance of these methods in terms of phase noise is comparable to the OPLL system. A key advantage of these approaches in [26,27] is that an optical modulator with a maximum operating frequency of 15 GHz can generate a millimeter-wave signal up to 60 GHz.

Disadvantage of the $2f$ and $4f$ methods

The main disadvantage of these techniques is that both approaches use optical filters to select the two optical sidebands. Another disadvantage is that in order to generate tunable mm-wave signals, a tunable optical filter must be used. These two disadvantages significantly increase the complexity and the cost of the system.

2.1.5. Microwave generation using a dual-wavelength laser

Microwave signals can also be generated using a dual wavelength laser source with the two wavelengths separated at a desired frequency [29]. It is different from the techniques of optical injection locking and the OPLL because, the two wavelengths from a dual wavelength laser source are not locked in phase. However, due to the fact that the two wavelengths are generated inside same cavity, the phase correlation between the two wavelengths is better than that using two free-running laser sources. To ensure that the two wavelengths are in single-longitudinal mode, a dual-band filter with ultra-narrow passbands must be used, thus, limiting the number of longitudinal modes to one in each passband. In the experimental demonstration [29], the ultra-narrow dual-band filter was a dual-wavelength ultra-narrow transmission band FBG with two ultra-narrow transmission bands, which was designed and fabricated based on the equivalent phase-shift (EPS) technique [30].

Advantages

The advantage of using a dual-wavelength laser source to generate a microwave or mm-wave signal is that the system is simpler with no need for a microwave reference source, which can significantly reduce the system cost. Due to the fact that the two wavelengths are generated from the same cavity, the phase correlation between the two wavelengths is better

than that using two free-running laser sources. The spectral width of the generated microwave signals is as small as 80 kHz with frequency stability better than 1 MHz in the free-running mode at room temperature.

Disadvantages

Due to the fact that three dual-wavelength ultranarrow transmission-bands can be incorporated into the laser cavity by using this technique, then microwave signals continuously tuned can not be generated.

3. Relaxation oscillation frequency

The relaxation oscillation frequency is the frequency of the quasi-sinusoidal oscillations around the steady state output power amplitude that occur during the disturbance of a continuously operating laser. Such oscillations are characterized by exponential damping. The phenomenon of relaxation oscillations has an effect on the performance of an unmodulated laser as well, by producing sidebands in the field fluctuation spectrum. They may be found directly from a small-signal measurement. Figure 7 illustrates the typical standard setup which is used for characterization of laser diodes. We assume that the laser diode is excited by an AC current source with amplitude I_1 and electrical frequency ω , biased at the constant current I_0 by means of a bias-tee. The modulated laser output is coupled into an optical fiber and then into a semiconductor PIN diode, biased through a simple bias network. The detected signal is fed into a spectrum analyzer.

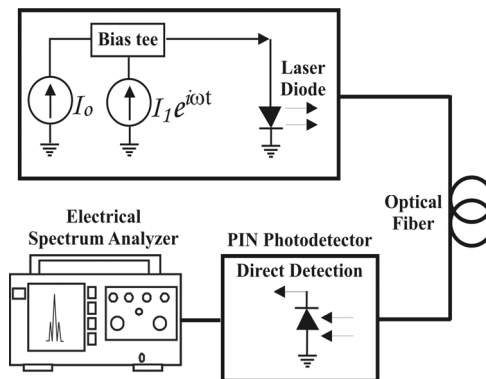


Figure 7. Typical experimental setup for measurement of relaxation oscillation frequencies of laser diodes.

3.1. Analysis of relaxation oscillation frequency

The employed physical model for analyzing the harmonic power can be explained by considering the small signal modulation analysis where the total electric current injected into the laser diode is given by:

$$I = I_0 + I_1 e^{j\omega t} \quad (3)$$

If photon and electron densities inside the active region of a semiconductor laser are denoted, respectively, by N_p and N_E , then expanding N_p and N_E as a Fourier series we find that these densities can be written as:

$$N_E = \sum_{n=0}^{\infty} N_{En} e^{jn\omega t} \quad (4)$$

$$N_p = \sum_{n=0}^{\infty} N_{pn} e^{jn\omega t} \quad (5)$$

where N_{pn} and N_{En} are the corresponding expansion coefficients of the photon and electron densities, respectively. On the other hand, the well-known rate equations for a single mode laser diode are [31]

$$\frac{dN_E}{dt} = \eta_i \frac{I}{qV} - \frac{N_E}{\tau_e} - V_g a (N_E - N_{tr}) N_p \quad (6)$$

$$\frac{dN_p}{dt} = \Gamma V_g a (N_E - N_{tr}) N_p - \frac{N_p}{\tau_p} \quad (7)$$

here η_i is the efficiency coefficient; τ_e is the carrier lifetime; a is the differential gain; N_{tr} is the threshold electron density; Γ is the cavity confinement factor; V_g is the cavity volume; and τ_p is the photon lifetime. In order to obtain information related with harmonic contents in optical output power of a laser diode, it is necessary to start our approach by substituting Eqs. (3) to (5) in Eq. (6) which results in

$$\begin{aligned} j\omega \sum_{n=1}^{\infty} N_{En} n e^{jn\omega t} &= \eta_i \frac{I_0 + I_1 e^{j\omega t}}{qV} - \frac{1}{\tau_e} \sum_{n=0}^{\infty} N_{En} e^{jn\omega t} \\ &\quad - V_g a \left(\sum_{n=0}^{\infty} N_{En} e^{jn\omega t} - N_{tr} \right) \sum_{n=0}^{\infty} N_{pn} e^{jn\omega t} \end{aligned} \quad (8)$$

In a similar way, if we substitute Eqs. (4) and (5) in Eq. (7) we obtain

$$\begin{aligned} j\omega \sum_{n=1}^{\infty} N_{pn} n e^{jn\omega t} &= \Gamma V_g a \left(\sum_{n=0}^{\infty} N_{En} e^{jn\omega t} - N_{tr} \right) \sum_{n=0}^{\infty} N_{pn} e^{jn\omega t} \\ &\quad - \frac{1}{\tau_p} \sum_{n=0}^{\infty} N_{pn} e^{jn\omega t} \end{aligned} \quad (9)$$

From DC Analysis ($n = 0$), however, we have:

$$N_{E_0} = \frac{\eta_i \frac{I_0}{qV} + V_g a N_{tr} N_{P_0}}{\frac{1}{\tau_e} + V_g a N_{P_0}} \quad (10)$$

$$\frac{1}{\Gamma \tau_p} = V_g a (N_{E_0} - N_{tr}) \quad (11)$$

The first harmonic of the photon density is generated directly by the first harmonic of the current applied to the laser diode, and we easily obtain [32]

$$N_{E_1} = \frac{\eta_i \frac{I_1}{qV}}{j\omega + \frac{1}{\tau_e} + V_g a N_{P_0} \left(1 + \frac{1}{j\omega \tau_p} \right)} \quad (12)$$

$$N_{P_1} = \frac{\Gamma V_g a N_{P_0} N_{E_1}}{j\omega} \quad (13)$$

Higher harmonics are found from recursive equations which in the general case for an arbitrary integer, $k > 1$, may be written as:

$$jk\omega N_{E_k} = -\frac{N_{E_k}}{\tau_e} - V_g a \left[(N_{E_0} - N_{tr}) N_{P_k} + N_{E_k} N_{P_0} + \sum_{n=1}^{k-1} N_{E_n} N_{P_{k-n}} \right] \quad (14)$$

$$jk\omega N_{P_k} = \Gamma V_g a \left(N_{E_k} N_{P_0} + \sum_{n=1}^{k-1} N_{E_n} N_{P_{k-n}} \right) \quad (15)$$

Hence, the k th harmonic of the photon density may be calculated once all the lower harmonics of photon and electron densities are known. If we define M_k as the parameter which relates the k th harmonic to the lower ones [33]

$$M_k = \sum_{n=1}^{k-1} N_{E_n} N_{P_{k-n}} \quad (16)$$

Therefore, we can find the k th harmonics of photon and electron densities as

$$N_{E_k} = \frac{-V_g a \left(1 + \frac{1}{jk\omega \tau_p} \right)}{jk\omega + \frac{1}{\tau_e} + V_g a N_{P_0} \left(1 + \frac{1}{jk\omega \tau_p} \right)} M_k \quad (17)$$

$$N_{P_k} = \frac{\Gamma V_g a}{jk\omega} (N_{P_0} N_{E_k} + M_k) \quad (18)$$

The frequency, ω_{RO} , at which the amplitude of the power harmonic content reaches its maximum is called the Relaxation Resonant Frequency. From Eqs. (12) and (13), the primary harmonic of the photon density is obtained as [32]

$$N_{P_1} = \frac{\Gamma V_g a N_{P_0}}{j\omega} \frac{\eta_i \frac{I_1}{qV}}{j\omega + \frac{1}{\tau_e} + V_g a N_{P_0} \left(1 + \frac{1}{j\omega\tau_p}\right)} \quad (19)$$

On the other hand, if the optical output power for the k th harmonic is given by $P_k = P_{outk} = \frac{hvV_p}{\tau_m} N_{pk}$, where τ_m is the mirror loss time, V_p represents the cavity volume and hv is the energy per photon, then by using this last equation we can obtain the optical output power for the first harmonic, written as

$$P_1(j\omega) = \frac{hvV_p}{\tau_m} \left(\frac{\Gamma V_g a N_{P_0} \eta_i \frac{I_1}{qV}}{-\omega^2 + \frac{j\omega}{\tau_e} + \frac{V_g a N_{P_0}}{\tau_p} (j\omega\tau_p + 1)} \right) \quad (20)$$

The cavity confinement factor, Γ , is equal to the ratio, V/V_p ; therefore, the above can be written as:

$$\frac{P_1(j\omega)}{I_1(j\omega)} = \frac{hvV_g a N_{P_0} \eta_i \frac{1}{\tau_m q}}{-\omega^2 + \frac{j\omega}{\tau_e} + \frac{V_g a N_{P_0}}{\tau_p} (j\omega\tau_p + 1)} \quad (21)$$

By separating the real and imaginary parts of the denominator of Eq. (21), we finally get [33]

$$\frac{P_1(j\omega)}{I_1(j\omega)} = \frac{hvV_g a N_{P_0} \eta_i \frac{1}{\tau_m q}}{\frac{V_g a N_{P_0}}{\tau_p} - \omega^2 + j\omega \left(\frac{1}{\tau_e} + V_g a N_{P_0} \right)} \quad (22)$$

This expression clearly has two poles at:

$$\omega = \pm \left[\frac{1}{\tau_p} V_s a N_{P_0} - \frac{1}{4} \left(\frac{1}{\tau_e} + V_s a N_{P_0} \right)^2 \right]^{\frac{1}{2}} + j \frac{1}{2} \left(\frac{1}{\tau_e} + V_s a N_{P_0} \right) \quad (23)$$

which are located in the first and second quadrants of the complex ω plane. We now notice that the real part of the denominator of Eq. (22) becomes zero at the frequency:

$$\omega = \omega_{RO}^2 = \frac{V_s a N_{P_0}}{\tau_p} \quad (24)$$

where $\omega_{RO} = 2\pi f_{RO}$. Since usually $\frac{1}{\tau_p} + V_s a N_{P_0} \ll \omega_{RO}$ holds, we conclude that the magnitude of Eq. (22) also reaches a maximum when $\omega \approx \omega_{RO}$. Hence, the denominator becomes purely imaginary, and the primary power harmonic content reaches its resonance mode. The optimum modulation frequency is the resonant frequency, which is determined from the bias current. Therefore, the optimal operation point for modulation where the power of the primary harmonic reaches its maximum must lie on the curve obtained from the following [34].

$$\omega_{RO} = \sqrt{\frac{V_s a}{q V_p} \eta_i (I_0 - I_{th})} \quad (25)$$

From the laser rate equations it is clear that the relaxation oscillation frequency should be proportional to the square root of the difference of the injection current and the threshold current. Thus, from Eq. (25) we can see that there is a linear relationship between relaxation oscillation frequency and the square root of the difference between the injection current and the threshold current. On the other hand, when the laser current density is lightly increased above its threshold value, the laser output power may be written as [35].

$$P_o = \eta_d (I_{in} - I_{th}) \frac{1.24}{\lambda_o} \quad (26)$$

where $\eta_d \frac{1.24}{\lambda_o}$ is called the differential responsivity of the laser (W/A).

4. Operation principle of direct detection

When a laser is biased in the threshold current region as shown in Figure 8, the laser intensity presents oscillations know as relaxation frequencies and can be seen as sidebands on both sides of the main laser line. In this case the electric field emitted by the laser diode can be represented as a directly modulated optical signal. After passing through an optical fiber, the optical field incident on the PD can be expressed as [36, 37]

$$E(t) = E_o \cos(2\pi f_o t) + E_{RO} \cos 2\pi(f_o + f_{RO})t + E_{RO} \cos 2\pi(f_o - f_{RO})t \quad (27)$$

Where f_o is the optical frequency of the main laser line, and both $f_o + f_{RO}$ and $f_o - f_{RO}$ represent optical sidebands. This method of detecting optical fields as shown in Figure 8 is called direct detection.

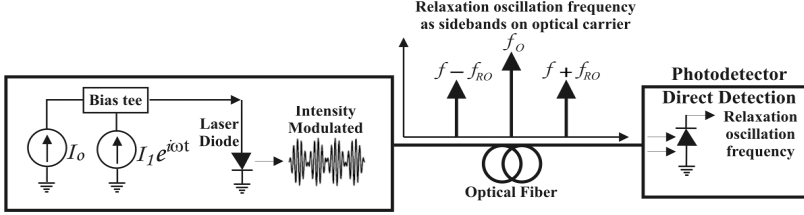


Figure 8. Direct detection to generate relaxation oscillation frequency when laser is operated in low threshold region.

The photo-detector responds to the power in the total field that it collects. The photo-current generated in the detector is proportional to the squared magnitude of the field and it is given by [38]

$$i(t) = \Re |E(t)|^2 = \Re P(t) \quad (28)$$

where $P(t)$ is the optical power and \Re is the detector responsivity given by [38]

$$\Re = \frac{\eta q}{h\nu} [A/W] \quad (29)$$

Where η ($0 < \eta \leq 1$) is the detector quantum efficiency, the parameters q and $h\nu$ are electronic charge (1.6021×10^{-19} C) and photon energy ($h = 6.6256 \times 10^{-34}$ J, $\nu = c/\lambda$) respectively. Substituting Eq. (27) into Eq. (28), and by using trigonometric identities, we obtain

$$\begin{aligned} i(t) &= \Re \left| E_o \cos(2\pi f_o t) + E_{RO} [\cos 2\pi(f_o + f_{RO})t + \cos 2\pi(f_o - f_{RO})t] \right|^2 \\ &= \frac{E_o^2}{2} + E_{RO}^2 + \frac{E_o^2}{2} \cos^2 2\pi(2f_o t) + 2E_o E_{RO} \cos 2\pi(f_{RO})t \\ &\quad + E_o E_{RO} [\cos 2\pi(2f_o + f_{RO})t + \cos 2\pi(2f_o - f_{RO})t] + \frac{E_{RO}^2}{2} \cos 2\pi(2f_o - 2f_{RO})t \\ &\quad + \frac{E_{RO}^2}{2} \cos 2\pi(2f_o + 2f_{RO})t + E_{RO}^2 [\cos 2\pi(2f_o)t + \cos 2\pi(2f_{RO})t] \end{aligned} \quad (30)$$

Notice that there are many terms in the detected signal expression where the PD cannot follow currents that are varying at $2f_o$, $2f_o + f_{RO}$, $2f_o - f_{RO}$, $2f_o + 2f_{RO}$ and $2f_o - 2f_{RO}$ so these currents average to zero. The average current from the PD will consist of four terms.

$$i(t) = \Re \left[\frac{E_o^2}{2} + E_{RO}^2 + 2E_o E_{RO} \cos 2\pi(f_{RO})t + E_{RO}^2 \cos 2\pi(2f_{RO})t \right] \quad (31)$$

The photo-current generated at the PD is found in a similar way as

$$i(t) = \Re \left[\frac{P_o}{2} + P_{RO} + 2\sqrt{P_o P_{RO}} \cos 2\pi(f_{RO})t + P_{RO} \cos 2\pi(2f_{RO})t \right] \quad (32)$$

The first two terms correspond to DC photo-currents and contain no information, but they do contribute to the shot noise of the signal detected. The next two terms correspond to the signal information which contains the relaxation oscillation frequency f_{RO} and its harmonic located at $2f_{RO}$.

5. Microwave photonic link by using external modulation

The photonic link described in this section is shown in Figure 9. The optical source is a continuous-wave DFB laser, followed by an EDFA. Amplified light is launched into the MZ-IM. Microwave modulation is imposed on the optical carrier through the MZ-IM.

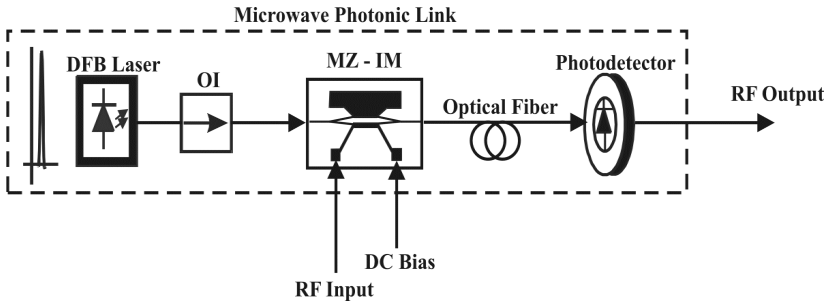


Figure 9. Microwave photonic link.

The modulated signal passes through optical fiber and is then incident upon the photodetector. Photodetector output can be connected to a microwave spectrum analyzer to observe gain, noise figure, and distortion of the microwave signal obtained at the end of the link.

For a modulator with half-wave voltage of V_π , signal voltage V , input power P_{in} , and insertion loss α , the modulated output power can be written [39, 40]

$$P_{out} = \frac{\alpha P_{in}}{2} \left[1 + \cos \left(\frac{\pi V}{V_\pi} \right) \right] \quad (33)$$

This expression can be examined in more detail by separating the signal voltage into a DC bias, V_b , and a modulation voltage, V_m .

$$P_{out} = \frac{\alpha P_{in}}{2} \left[1 + \cos \left(\frac{\pi V_b}{V_\pi} + \frac{\pi V_m}{V_\pi} \right) \right] \quad (34)$$

Using a trigonometric identity for the sum of cosines, the output power can be rewritten as:

$$P_{out} = \frac{\alpha P_{in}}{2} \left[1 + \cos \left(\frac{\pi V_b}{V_\pi} \right) \cos \left(\frac{\pi V_m}{V_\pi} \right) - \sin \left(\frac{\pi V_b}{V_\pi} \right) \sin \left(\frac{\pi V_m}{V_\pi} \right) \right] \quad (35)$$

Typically, the DC bias point of the MZ-IM is chosen to bring the modulator into quadrature. This is accomplished by operating at $V_b = V_\pi / 2$. At this bias voltage, the transfer curve is linear and even order harmonics are suppressed.

Deviation from the quadrature bias point can be described by an angle ϕ .

$$P_{out} = \frac{\alpha P_{in}}{2} \left[1 + \cos \left(\frac{\pi}{2} + \phi \right) \cos \left(\frac{\pi V_m}{V_\pi} \right) - \sin \left(\frac{\pi}{2} + \phi \right) \sin \left(\frac{\pi V_m}{V_\pi} \right) \right] \quad (36)$$

$$P_{out} = \frac{\alpha P_{in}}{2} \left[1 - \sin \phi \cos \left(\frac{\pi V_m}{V_\pi} \right) - \cos \phi \sin \left(\frac{\pi V_m}{V_\pi} \right) \right] \quad (37)$$

At $\phi = 0$, $V_b = V_\pi / 2$ and the modulator is in quadrature. This corresponds to the typical linear transmission regime for an electro-optic modulator. The quadrature output power from the modulator is denoted by P_Q .

$$P_Q = \frac{\alpha P_{in}}{2} \left[1 - \sin \left(\frac{\pi V_m}{V_\pi} \right) \right] \quad (38)$$

For single applications, the DC bias point of the MZ-IM can be shifted away from the quadrature point. Even-order distortion is increased, but these terms lie outside the frequency range of interest. As the bias point is shifted, shot noise falls linearly with transmission and RIN is reduced quadratically. However, the link gain is only reduced at the rate of $\sin^2 \phi$. For links dominated by RIN, shifting the bias point toward the transmission null reduces the link noise figure. This improvement continues until the shot noise limit is reached. Consider a MZ-IM biased near $\phi = 90^\circ$. This corresponds to an operating regime with reduced output power. For simplicity, let $\phi = 90^\circ - \delta$ so that $\phi = 0^\circ$ corresponds to the quadrature operating point and $\delta = 0^\circ$ corresponds to the transmission null. These operating regimes and angles are summarized graphically in Figure 10.

By substituting δ for $\pi/2 - \phi$, the modulator output power can be written as [40]

$$P_{out} = \frac{\alpha P_{in}}{2} \left[1 - \cos \delta \cos \left(\frac{\pi V_m}{V_\pi} \right) - \sin \delta \sin \left(\frac{\pi V_m}{V_\pi} \right) \right] \quad (39)$$

The first bracketed term represents continuous wave output power. The second term contains even-order harmonic components. The third term contains the linear signal of interest as well as odd-order harmonic components. Note that for $\delta = 90^\circ$, $P_{out} = P_Q$ as expected. For $\delta \ll 1$, the output power can be approximated by using a Taylor series expansion to replace $\sin \delta$ with δ and $\cos \delta$ with $1 - \delta^2/2$.

$$P_{out} \approx \frac{\alpha P_{in}}{2} \left[1 - \left(1 - \frac{\delta^2}{2} \right) \cos \left(\frac{\pi V_m}{V_\pi} \right) - \delta \sin \left(\frac{\pi V_m}{V_\pi} \right) \right] \tag{40}$$

The harmonic components can be identified by assuming small signal operation with $\pi V_m/V_\pi \ll 1$. For the cosine function, the Taylor series expansion can be truncated after the first term. This truncation is justified by operating the modulator over a single octave so that even-order distortion can be neglected.

$$P_{out} \approx \frac{\alpha P_{in}}{2} \left[1 - \left(1 - \frac{\delta^2}{2} \right) - \delta \sin \left(\frac{\pi V_m}{V_\pi} \right) \right] \tag{41}$$

The sine term can be expressed using a third-order Taylor series expansion.

$$P_{out} \approx \frac{\alpha P_{in}}{2} \left\{ \frac{\delta^2}{2} - \delta \left[\frac{\pi V_m}{V_\pi} - \frac{1}{6} \left(\frac{\pi V_m}{V_\pi} \right)^3 \dots \right] \right\} \tag{42}$$

From this expression, it can be seen that the DC term decreases more rapidly than the modulation term for a given increase in δ . By shifting the DC bias point away from quadrature, carrier suppression can be achieved. This can create a double sideband suppressed carrier (DSB-SC) modulation format.

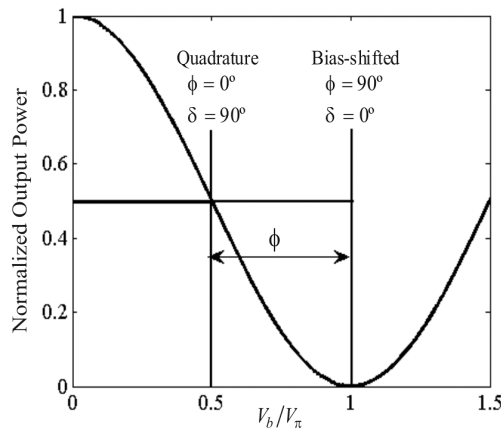


Figure 10. Quadrature and bias-shifted operating regimes.

6. Passive components for microwave photonics

This section presents an overview of the passive components for microwave photonics such as optical fiber, optical isolator, polarization control and optical fiber couplers.

6.1. Optical fiber

The optical fibers used in analog photonic links have a very simple structure. They consist of two sections: the glass core and the cladding layer as shown in Figure 11. The core is a cylindrical structure, and the cladding is a cylinder without a core. Core and cladding have different refractive indices, with the core having a refractive index, n_1 , which is slightly higher than that of the cladding, n_2 . This difference in refractive indices enables the fiber to guide the light. Because of this guiding property, the fiber is also referred to as an “optical waveguide.” Besides these two sections there is also a further layer known as the secondary cladding that does not participate in the propagation but gives the fiber a minimum level of protection.

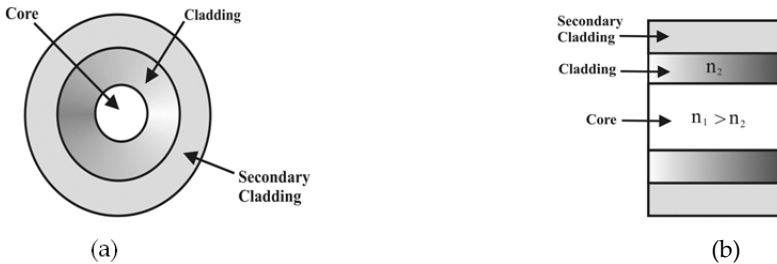


Figure 11. Typical optical fiber (a) cross section, (b) longitudinal cross section.

The basics of light propagation can be discussed with the use of geometric optics. The basic law of light guidance is Snell’s law as shown in Figure 12(a). Consider two dielectric media with different refractive indices and with $n_1 > n_2$ and that are in perfect contact. At the interface between the two dielectrics, the incident and refracted rays satisfy Snell’s law of refraction and can be written by

$$n_1 \sin \phi_1 = n_2 \sin \phi_2 \quad (43)$$

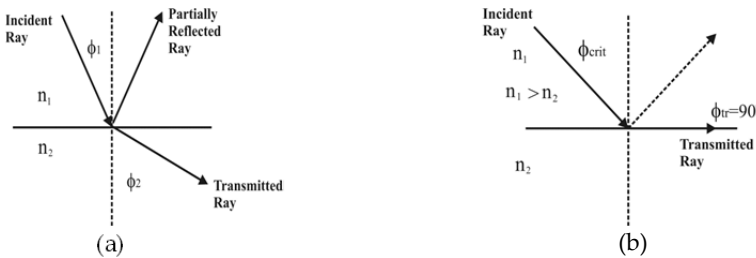


Figure 12. Snell’s law, (a) showing transmitted ray, (b) showing total reflection when critical angle is achieved.

In addition to the refracted ray there is a small amount of reflected light in the medium with refractive index n_1 . Because $n_2 < n_1$ then always $\phi_2 > \phi_1$. As the angle of the incident ray increases there is an angle at which the refracted ray emerges parallel to the interface between the two dielectrics as shown in Figure 12(b). This angle is known as the critical angle, ϕ_{crit} , and from Snell's law is given by

$$\phi_{crit} = \sin^{-1}\left(\frac{n_2}{n_1}\right) \tag{44}$$

For a ray to be launched into the fiber and propagated, it must arrive at the interface between the two media (with different refractive indices) at an angle that is at minimum equal to ϕ_{crit} . Figure 13 illustrates the geometry for the derivation of the acceptance angle. To satisfy the condition for total internal reflection, the ray arriving at the interface between the fiber and outside medium, like air, must have an angle of incidence less than θ_{acc} , otherwise the internal angle will not satisfy the condition for total reflection, and the energy of the ray will be lost in the cladding. From Snell's law at the interface we obtain

$$n_0 \sin\theta_1 = n_1 \sin\theta_2 \tag{45}$$

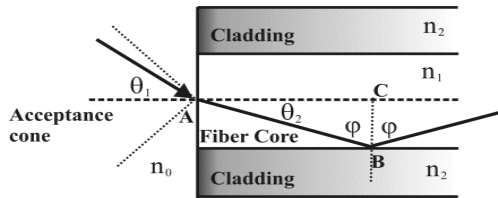


Figure 13. Geometry for the derivation of the acceptance angle.

From the right triangle ABC in Figure 13, the angle $\phi = \pi/2 - \theta_2$. Substituting θ_2 into Eq. (45), we obtain

$$n_0 \sin\theta_1 = n_1 \cos\phi \tag{46}$$

In the limit as the incident angle, θ_1 approaches θ_{acc} , the internal angle approaches the critical angle for total reflection, ϕ_{crit} . Then, by introducing the trigonometric relation $\sin^2\phi + \cos^2\phi = 1$ into Eq. (46), we obtain

$$n_0 \sin\theta_1 = n_1 \cos\phi = n_1 (1 - \sin^2\phi)^{1/2} = n_1 \left(1 - \left(\frac{n_2}{n_1}\right)^2\right)^{1/2} = (n_1^2 - n_2^2)^{1/2} \tag{47}$$

This equation defines the angle within which the fiber can accept and propagate light and is known as the "Numerical Aperture" (NA).

$$NA = n_o \sin \theta_{acc} = (n_1^2 - n_2^2)^{1/2} \quad (48)$$

This equation states that for all angles of incident where the inequality $0 \leq \theta_1 \leq \theta_{acc}$ is satisfied, the incident ray will propagate within the fiber. The parameter NA expresses the propensity of the fiber to accept and propagate light within the solid cone defined by an angle, $2\theta_{acc}$. The equation for the NA can be also expressed in terms of the fractional change in the index of refraction of core and cladding Δ . This refractive index difference is given by

$$\Delta = \frac{n_1^2 - n_2^2}{2n_1^2} \approx \frac{n_1 - n_2}{n_1} \quad (49)$$

With these simplifications the NA can now be written as

$$NA = n_1 (2\Delta)^{1/2} \quad (50)$$

6.1.1. Attenuation in fiber

Attenuation in optical fiber leads to a reduction of the signal power as the signal propagates over some distance. When determining the maximum distance that a signal can propagate for a given transmitter power and receiver sensitivity, one must consider attenuation. Let $P(L)$ be the power of the optical pulse at distance L km from the transmitter and α_{fiber} be the attenuation constant of the fiber (in dB/km). Attenuation is characterized by [41]

$$P_R(L) = 10^{-\alpha_{fiber} L/10} P_T(0) \quad (51)$$

Where $P_T(0)$ is the optical power at the transmitter and the received optical power for a link length of L km, is $P_R(L)$. The maximum distance between the transmitter and the receiver depends more heavily on the constant α_{fiber} than on the optical power launched by the transmitter. This distance is given by

$$L_{max} = \frac{10}{\alpha_{fiber}} \log_{10} \frac{P_T(0)}{P_R} \quad (52)$$

6.2. Optical isolator

An isolator inside an optical fiber link allows the propagation of the light in only one direction (from left to right as is indicated in Figure 14), with minimum loss, avoiding reflected light in sense inverse. Depending on the design, the reflected optical signal has an attenuation value of 40 to 70 dB [42].

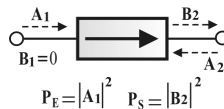


Figure 14. Scheme and flux of signals across an optical isolator.

The optical isolator is a network of 2 ports, and as such, it can be described by a scattering matrix 2x2

$$S = \begin{pmatrix} S_{11} & S_{12} \\ S_{21} & S_{22} \end{pmatrix} \tag{53}$$

This device is characterized by two parameters: the insertion losses (L), and the isolation relationship (I), both expressed in dB. These parameters are related by the optical power at the input and the output of the device, the optical fields in their two ports, and their scattering parameters by means of the following relationships:

$$L = 10\text{Log}\left(\frac{P_E}{P_S}\right) = 10\text{Log}\left(\frac{1 - |S_{11}|^2}{|S_{21}|^2}\right) \tag{54}$$

$$I = 10\text{Log}\left(\frac{|A_2|^2}{|B_1|^2}\right) = 10\text{Log}\left(\frac{1}{|S_{12}|^2}\right) \tag{55}$$

In an ideal isolator, insertion losses are $L = 0$ dB, and the isolation relationship is $I = \infty$. Generally, optical isolators are placed at the output of the optical sources in order to avoid reflections of light from returning back to the source avoiding in this way instabilities. Furthermore, isolators are used by the Doped Fiber Amplifiers with the aim of avoiding an oscillating behavior. Figure 15 illustrates a basic diagram of an optical isolator and is used to explain the basic operation of this device [43]. Light propagating from left to right is linearly polarized by means of a vertical polarizer "A" placed at the input port of the isolator. Then the polarization plane of the light is rotated 45° by means of a polarization rotator. Finally, the light is transmitted through a linear polarizer "B" whose axis forms an angle of 45° in relation to the axis of the polarizer "A". The reflecting signal (light propagating from right to left), is linearly polarized into the polarizer "B" 45° with respect to the axis of the polarizer "A". Subsequently, a rotation of the plane of linear polarization at 45° is made, and by consequence at the input of the polarizer "A," its polarization plane forms an angle of 90° (orthogonal) with its axis of polarization. By consequence, the light is blocked.

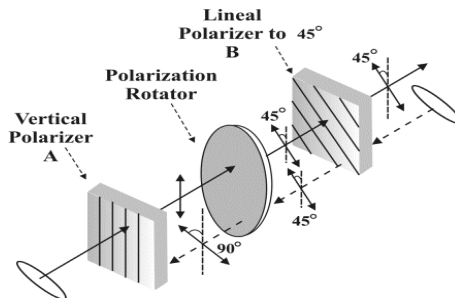


Figure 15. Principle of operation of an optical isolator.

6.3. Polarization rotator

A polarization rotator rotates the polarization plane of an optical field linearly polarized at its input at an angle θ [43]. If the input signal is an optical field linearly polarized forming an angle θ_1 with the axis x , then the Jones Matrix can be expressed as

$$J = \begin{bmatrix} \cos \theta_1 \\ \sin \theta_1 \end{bmatrix} \quad (56)$$

The output signal is an optical field linearly polarized forming an angle θ_2 , and by consequence the Jones matrix corresponding to the rotator is given as

$$M = \begin{bmatrix} \cos \theta & -\sin \theta \\ \sin \theta & \cos \theta \end{bmatrix} \quad (57)$$

where: $\theta = \theta_2 - \theta_1$.

6.4. Polarization control

A polarization control changes the polarization state of the light. Currently in the systems, the polarization controls can be inserted in the arms of an optical signal or in the arms of a signal of an optical local oscillator in order to maintain or to match the polarization state of both signals. Figure 16 shows a scheme corresponding to a polarization control. Basically, this scheme is composed of a monomode optical fiber crossing three plates. The optical fiber (from left to right in the figure) is rolled in a circular way one time in the first plate, 2 times in the second plate, and finally 1 time in the third plate.

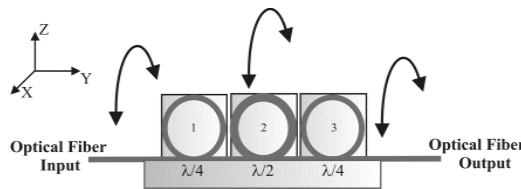


Figure 16. Polarization Control.

For a particular wavelength and an appropriate diameter of the plates, phase changes are introduced in the incident optical field due to the stress applied to the optical fiber, and by consequence, a birefringence is induced. The birefringence degree is function of the material of which the optical fiber, the plate diameter, and the cladding diameter of the optical fiber is composed, and it is defined as [44]

$$\Delta n = \alpha (r / R)^2 \quad (58)$$

where α is a parameter related to the fiber material, r is the cladding diameter, and R is the plate diameter defined

$$R = 8\pi ar^2 / \lambda \quad (59)$$

When an optical field is propagated by the fiber control, this field will suffer a phase change of 90° at the output of the first plate, and by consequence this plate has a similar behavior as a retarder plate of $\lambda/4$ [44]. The second plate acts as a retarder plate of $\lambda/2$ because at the output the optical field has a phase change of 180° . This phase change can be expressed as [44].

$$\Delta\phi = (2\pi / \lambda)\Delta n 2\pi R \quad (60)$$

Taking into account this effect and assuming that the incident optical field has an elliptical polarization state, the first retarder plate $\lambda/4$ changes this polarization state to a lineal polarization state. The second retarder plate $\lambda/2$ rotates the polarization state toward a specific direction. Finally, the third plate $\lambda/4$ changes the linear polarization into a desired polarization state.

6.5. Optical fiber couplers

The optical system communications requires devices capable of coupling light from one fiber or various fibers to others. Typically, this coupling of light has been achieved by using beam splitters fabricated on bulk devices. However, for the case of guided signal transmission this task can be achieved by using couplers [45]. A coupler is a passive device capable of distributing energy from M input guides to N output guides [45]. In this sense, two technologies have been developed to fabricate couplers. One of these is based on optical fibers whereas the other is based on bulk optics, however the principles of operation are similar in both cases. Currently, the coupler most commonly used in optical system communications is the directional coupler 2×2 . Figure 17 illustrates a scheme of this type of coupler.

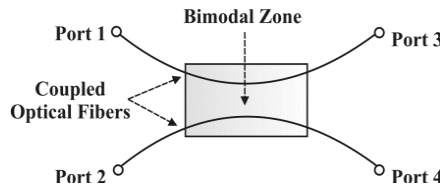


Figure 17. Scheme of an optical coupler 2×2 .

From this figure, it is clearly appreciable that this is a 4-port device. In technology of optical fibers, this device can be of two types: (a) Evanescent field [46, 47], and (b) Modal interference. In the first case, the evanescent mode corresponding to the fundamental mode of a guide is used to excite the apparition and propagation of the fundamental mode in another guide producing a controllable energy. In the second case, a common bimodal zone to both guides is generated obtaining in this way the transfer of energy by means of a controlled interference between the modes that are being propagated in this zone. The coupler of evanescent field is generated by placing two guides very near between them as is

illustrated in Figure 18(a). The evanescent field of the fundamental mode in one of the two guides is introduced and excites the apparition of the fundamental mode in the other guide whose evanescent field excites and causes a transfer of energy to the first guide. This process is produced in a continuous way generating a periodic signal exchange between the two guides [45].

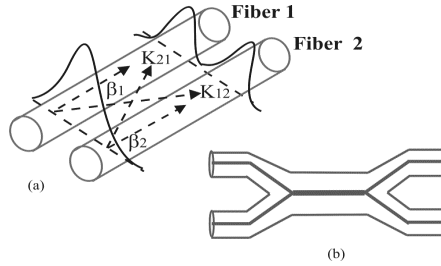


Figure 18. Transfer of energy in an evanescent field coupler (a). Diagram of a coupler based on a bimodal zone (b).

For the coupler based on modal interference, see Figure 18(b), the coupling zone is constituted by a common region of dimensions larger than the input and output of the guides allowing in this way the propagation of two modes (bimodal guide). The coupling energy between both produces the propagation of energy from one guide to another [45]. The analysis for these types of devices uses the coupling equations. There are two coupled modes that correspond to the fundamental modes of each guide. If $a_1(z)$ and $a_2(z)$ are the amplitudes corresponding to the fields of the fundamental modes of Guides 1 and 2, and β_1 and β_2 are the propagation constants (not necessarily equal), then the coupling equations between modes are for this case

$$\begin{aligned} \frac{da_1}{dz} &= -j\beta_1 a_1 + K_{12} a_2 \\ \frac{da_2}{dz} &= -j\beta_2 a_2 + K_{21} a_1 \end{aligned} \quad (61)$$

For the case of guides without losses, and taking into account the conservation principle of energy, $K_{12} = K_{21}^*$, where $K_{21} = jc$. The constant c is the coupling coefficient given as

$$c = \frac{K_{12}}{j} = \frac{\omega \varepsilon_0}{4P} \int_{-\infty}^{\infty} \int_{-\infty}^{\infty} (n^2(x, y) - n_2^2) E_1^t(x, y) E_2^t(x, y) dx dy \quad (62)$$

where ω is the angular frequency (rad/sec), P is the power, ε_0 is the permittivity in the free space, n_2 is the index refraction corresponding to the cladding of both fibers, $n(x, y)$ is the transversal variation of the index refraction corresponding to the zone where the guides are very near between them, and $E_1^t(x, y)$ and $E_2^t(x, y)$ are the transversal profiles corresponding to the fundamental modes for the Guides 1 and 2, respectively. To solve Eq. (61), it is necessary to use the parameter $\delta = (\beta_1 - \beta_2) / 2$. This parameter indicates the

difference between the guides that composes the coupler. The solution of (61) provides the values of the amplitudes of the electric field in any point z for both guides $a_1(z)$ and $a_2(z)$ in function of the values of the amplitudes of electric fields to its input $a_1(0)$ and $a_2(0)$. The solution can be expressed as a matrix [45]

$$\begin{pmatrix} a_1(z) \\ a_2(z) \end{pmatrix} = e^{-j\left(\frac{\beta_1 + \beta_2}{2}\right)z} \begin{pmatrix} A & jB \\ jB^* & A^* \end{pmatrix} \begin{pmatrix} a_1(0) \\ a_2(0) \end{pmatrix} \quad (63)$$

Where

$$A = \cos\left(z\sqrt{c^2 + \delta^2}\right) + j\delta \frac{\text{sen}\left(z\sqrt{c^2 + \delta^2}\right)}{\sqrt{c^2 + \delta^2}} \quad (64)$$

$$B = c \frac{\text{sen}\left(z\sqrt{c^2 + \delta^2}\right)}{\sqrt{c^2 + \delta^2}}$$

The phase factor $\exp-j\left(\frac{\beta_1 + \beta_2}{2}\right)z$ is a common factor, and so it is not necessary to be considered in subsequent calculations. In practice, optical fiber couplers are made using similar fibers, for this reason $\beta_1 = \beta_2 = \beta$ and $\delta = 0$. Consequently, the matrix relationship (63) is

$$\begin{pmatrix} a_1(z) \\ a_2(z) \end{pmatrix} = \begin{pmatrix} \cos(cz) & j\text{sen}(cz) \\ j\text{sen}(cz) & \cos(cz) \end{pmatrix} \begin{pmatrix} a_1(0) \\ a_2(0) \end{pmatrix} \quad (65)$$

Defining the coupling constant as $k = \text{sen}^2(cz)$, then (65) takes the form

$$\begin{pmatrix} a_1(z) \\ a_2(z) \end{pmatrix} = \begin{pmatrix} \sqrt{1-k} & j\sqrt{k} \\ j\sqrt{k} & \sqrt{1-k} \end{pmatrix} \begin{pmatrix} a_1(0) \\ a_2(0) \end{pmatrix} \quad (66)$$

Since the coupling constant k is generally variable with wavelength, the characteristics of the coupler may vary with the operating frequency. However, this effect can be utilized to create optical filters, multiplexers and wavelength demultiplexers [45]. The energy transfer process can easily be evaluated assuming that at the input of the coupler there is only signal in Guide 1, this is, $a_2(0) = 0$. From equation (65) it is possible to obtain the optical power in each guide for each value of z :

$$P_1(z) = |a_1(z)|^2 = P_1(0)\cos^2(cz) = P_1(0)(1-k) \quad (67)$$

$$P_2(z) = |a_2(z)|^2 = P_1(0)\text{sen}^2(cz) = P_1(0)k$$

A special case is when $k = 1/2$. In this case, the optical power in the input guide is divided equally between the two output guides of the coupler. The device is then called a 3 dB coupler.

Until now, the description of the coupler has been made on the assumption that it behaves ideally, this is, without considering losses. In practice this is not real, and from experimental as well as commercial points of view, it is necessary to define a set of parameters that allows the behavior of the coupler to be determined.

Coupling constant

$$k = \frac{P_4}{P_3 + P_4} \quad (68)$$

This constant indicates the optical power division between the output ports.

Excess Loss

$$\Gamma(dB) = 10\log(\gamma) = 10\text{Log} \left[\frac{P_1}{P_3 + P_4} \right] \quad (69)$$

This parameter provides the relationship between the total power at the input and the output power of the device.

Directivity coupler

$$D(dB) = 10\text{Log} \left[\frac{P_2}{P_1} \right] \quad (70)$$

This parameter indicates the fraction of input power that the coupler returns in the form of signal retro-propagated to Guide 2.

Insertion Losses

$$L_i(dB) = 10\text{Log} \left[\frac{P_1}{P_3} \right] \quad (71)$$

This parameter indicates the level of losses introduced by the coupler considering that the signal propagation is through a given configuration of the input port and the output port.

7. Experimental results

According to the theoretical descriptions explained in this chapter, we have assembled in the laboratory the proposed experimental setup shown in Figure 1. For the stage where relaxation oscillation frequencies were measured, we used two fiber-coupled DFB laser sources (Thorlabs, model S3FC1550) with a central wavelength of 1550 nm, a threshold current of ≈ 8 mA and a differential responsivity of 0.25 mW/mA. An optical isolator OI was connected to each DFB laser to avoid instabilities from feedback into the lasers, and an optical coupler was used to split the optical beam. In order to increase the power level of the microwave signal, it was necessary to connect an EDFA in one of the ports of the optical

coupler. After that, the amplified optical signal was launched to fast photodetector PD1 (MITEQ model DR-125G-A) which has a typical optical-to-electrical transfer gain (V/W) of 1900, and -3 dB bandwidth of 12.5 GHz. In order to measure the optical spectrum of the DFB laser, it was necessary to connect the other port of optical coupler to an OSA Anritsu model MS9710C. On the other hand, the obtained photo-current by photo-detector was measured by using an ESA, Agilent model E4407B.

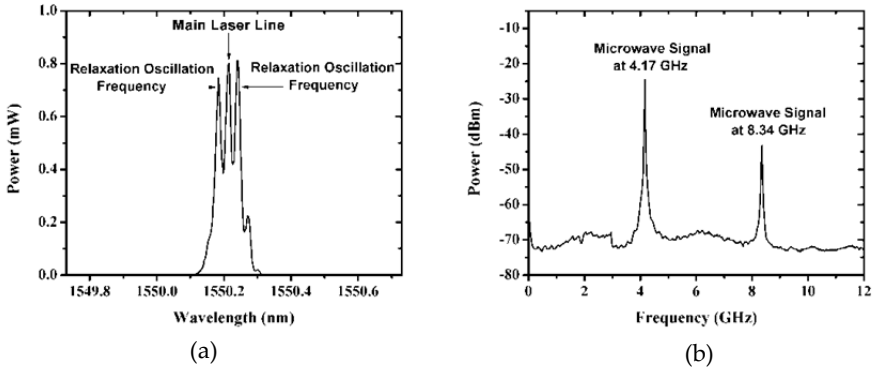


Figure 19. Measured spectra: (a) showing relaxation oscillation frequencies, (b) microwave signal by using direct detection.

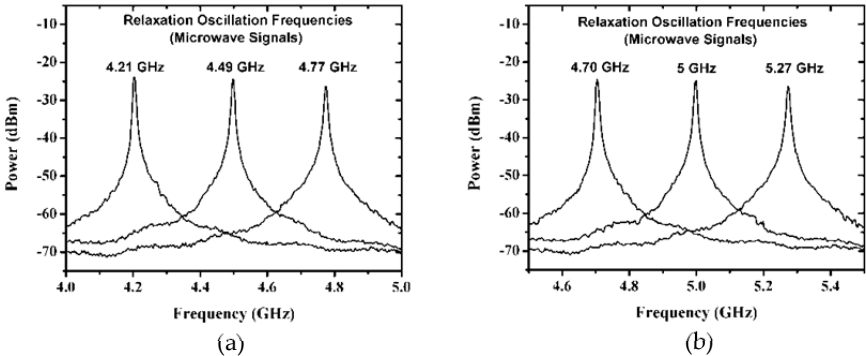


Figure 20. Microwave signal continuously tuned. (a) between 4 and 5 GHz, (b) between 4.5 and 5.5 GHz.

As can be seen from Figure 19(a), the optical spectrum of one of the lasers (DFB 1) exhibits sidebands on both sides of the main laser line as a result of it being biased in the threshold current region. In this case, its optical power was emitted at 1.15 mW at a temperature of 23.5° C. According to Eq. (26), the injection current was approximately at 12.6 mA. With these operation data, a microwave signal was obtained on C band by using direct detection, as shown in Figure 19(b). This spectrum shows a microwave signal located at 4.17 GHz and its harmonic located at 8.34 GHz. This result is in good agreement with Eq. (32). Similar

results were found with the DFB 2 laser when it was operated in the low laser threshold current region. Because of its linear relationship between relaxation oscillation frequency and the square root of the difference between the injection current and the threshold current as defined in Eq. (25), and since the optical power of each DFB laser can be tuned by using a power controller system which modifies the injection current through a laser diode correspondingly, we obtained several microwave signals located between 4 and 5 GHz for DFB 1 when it was tuned between 0.7 mW and 0.8 mW at a temperature of 25° C, as can be seen in Figure 20(a). Microwave signal were obtained between 4.5 and 5.5 GHz, when the optical power of DFB 2 was tuned between 0.9 mW and 1 mW with a temperature of 26° C as can be seen in figure 20(b).

To show a potential application in the field of communication systems of relaxation oscillation frequencies, we report herein the simultaneous multiplexed transmission of an analog TV signal of 67.25 MHz (TV channel 4) over a photonic link of 30 Km of optical fiber by using two microwave signals at 4 and 5 GHz. From the experimental setup illustrated in Figure 1, it can be seen that the obtained relaxation oscillation frequencies from the PD1 were mixed with a TV signal by using an electrical frequency mixer (Mini-Circuits, model ZX05-U72MH-s+). Then the obtained modulated signal as shown in Figure 21(a), was amplified and transmitted through a photonic link of 30 Km of optical fiber. Such microwave sub-carriers were applied to an electro-optic modulator which imprints the electric signal on the laser emission. The intensity-modulated optical signal of DFB 3 laser was then transmitted through the optical channel. After that, in the receiver, the transmitted information was photo-detected. The spectrum of the multiplexed microwave signal after photodetection is shown in Figure 21(b). The output electrical spectrums in Figure 21 clearly show the multiplexed microwave sub-carriers. The spectral separation is approximately 1 GHz. According to the experimental setup shown in Figure 1, the photo-detected signal is amplified, filtered and synchronously down-converted to recuperate the analog TV signal of 67.25 MHz. The resulting power spectral density was displayed in an electrical spectrum analyzer, where it was analyzed to measure the power level of recovered information.

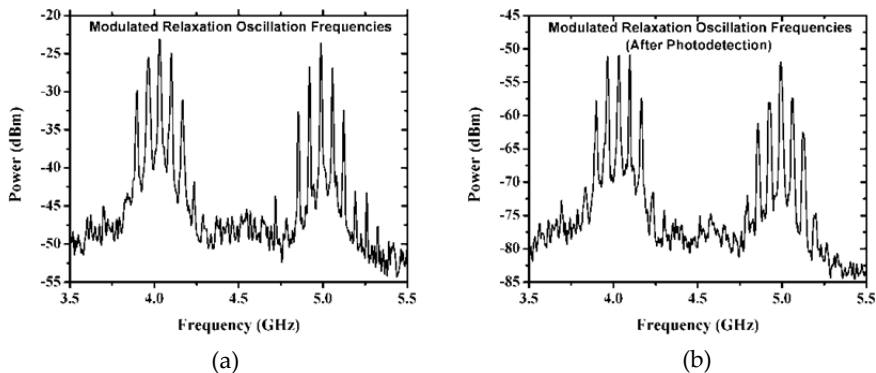


Figure 21. Modulated relaxation oscillation frequencies with a TV signal. (a) applied to electro-optic modulator, (b) after photodetection.

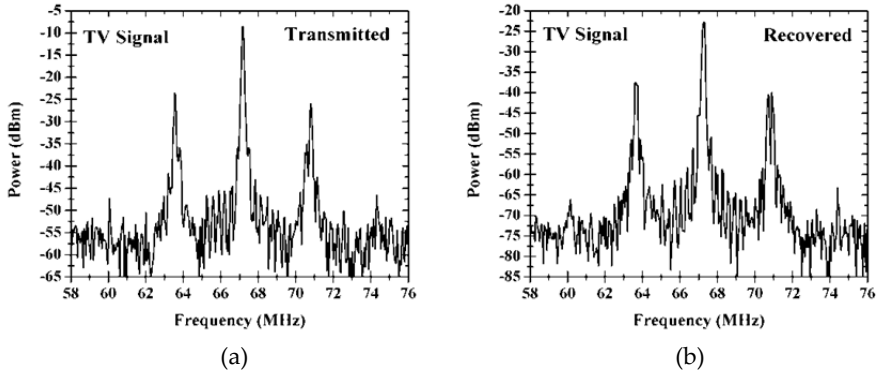


Figure 22. TV signals at 67.25 MHz, (a) transmitted (b) recovered.

Figure 22(a) shows the frequency spectrum of an analog NTSC TV signal at the input of the transmitter located at 67.25 MHz (before being applied to a frequency mixer). In Figure 22(b), we can see the obtained analog NTSC TV signal at the output of the receiver when the local oscillator was synchronized at 4 GHz. The analog information was successfully transmitted from the transmitter to the receiver, and the received signal was satisfactorily reproduced at the receiver without noticeable degradation compared the original NTSC TV signal. Before experimentally quantifying the parameter of SNR for both cases (TV transmitted and recovered in the proposed photonic link), it is essential to give an analysis of noise in terms of SNR.

7.1. SNR performance of an analog photonic link

To reconstruct a signal at the receiver faithfully, the noise power must be small compared to the signal level. In other words, the SNR is a figure of merit in characterizing a receiver circuit. There are three dominant noise sources on the optical receiver side of an analog photonic link: thermal noise, shot noise, and received relative intensity noise (RIN). The RIN are the fluctuations of the laser intensity caused by random spontaneous light emissions. In a PD, noise can be attributed primarily to two factors. The shot noise, also known as quantum noise, originates from the statistical nature of photon-to-electron conversion. Thermal noise, on the other hand, is an intrinsic property of any electrical circuit that is connected to the PD.

7.1.1. Shot noise

Photon-to-electron conversion is fundamentally a quantum mechanical process. When a photon is absorbed, a pair of electron-holes is generated. Therefore, the photo-generated current is not truly continuous but has a discrete nature. It fluctuates around some average value as a result of the discrete charge of the carriers that contribute to it. Because of the random nature of the current fluctuations, the noise current must be characterized in a statistical manner. It is common to describe the noise current by its mean square value. For a PIN detector, the mean square value of the shot noise is [48].

$$\sigma_s^2 = 2qI_pB \quad (72)$$

where I_p is the photo-current, q is the electron charge, and B is the bandwidth within which the noise is being measured. Eq. (72) implies that shot noise has a constant spectral density, an assumption that holds for all frequencies of interest. Normally, B is set by the bandwidth of the receiver. This shows that one way to minimize the effects of shot noise is to keep the bandwidth of circuit as narrow as possible. The current flowing through a PIN diode is not just photo-generated. Any reverse bias junction has a leakage current. For photo-detectors, the leakage current is called dark current I_D , because it exists even when there is no optical power. As a result, the mean square value of the total shot noise is given by

$$\sigma_s^2 = 2q(I_p + I_D)B \quad (73)$$

7.1.2. Thermal noise

Shot noise is a consequence of the quantum nature of light detection. Therefore, it is a fundamental property of the photo-detector and sets a maximum limit on the value of SNR. In such a case, the SNR is said to be quantumly limited. In reality, however, there are other sources of noise almost always present. Chief among these is thermal noise, also known as Johnson noise, associated with the electric circuits connected to the detector. The source of this noise is the thermal motion of electrons in the load resistor R_L . The mean squared of the thermal noise in the load resistor is given by

$$\sigma_T^2 = \frac{4kTB}{R_L} \quad (74)$$

where k is Boltzmann's constant, T is the absolute temperature, and B is bandwidth. Like shot noise, thermal noise has a constant spectral density. This is another reason to keep the bandwidth of a receiver as low as possible, i.e., just sufficient to pass the signals of interest.

7.1.3. Relative intensity noise

Any real laser has a certain amount of noise due to spontaneous emission. As a result both the amplitude and the phase are randomly varying in any real laser, then the wave front a DFB laser source may be represented by its electric field as

$$\bar{E}_1(t) = E_o(1 + V(t)) \exp j(2\pi\nu_o t + \varphi(t)) \quad (75)$$

where $V(t)$ and $\varphi(t)$ represent the amplitude and phase of the noise, respectively. If the field expressed in Eq. (75) is detected by a photo-detector with responsivity \mathfrak{R} , the resulting current is given by [49]

$$I = \mathfrak{R}E_o^2[1 + V(t)]^2 \quad (76)$$

Typically, the amplitude noise, $V(t)$, is very small so that Eq (76) can be rewritten as

$$I \approx \Re E_0^2 [1 + 2V(t)] \quad (77)$$

The noise term $2V(t)$ represents the RIN; it describes the laser power fluctuations. The power spectral density of the RIN is denoted by ζ ; it has the units of 1/Hz. The quantity $10 \log \zeta$ is known as the RIN.

$$RIN \equiv 10 \log \zeta, \text{ dB/Hz} \quad (78)$$

The typical values of RIN for a DFB laser are better than -155 dB/Hz. The power spectrum of the RIN is not flat, hence it is not a white noise source. In an analog photonic link, we use a photodiode to detect the optical power from the M-Z modulator. Thus, RIN can be expressed as [50].

$$RIN = \frac{\left(\frac{i_{RIND}}{\Re} \right)^2}{B \left(\frac{I_D}{\Re} \right)^2} = \frac{i_{RIND}^2}{BI_D^2} \quad (79)$$

From Eq. (79), we obtain the received mean square current RIN noise of the receiver as:

$$i_{RIND}^2 = RIN \cdot I_D^2 B \quad (80)$$

Comparatively, i_{RIND}^2 is proportional to I_D^2 , whereas the shot noise is linearly proportional to I_D . Therefore, the RIN noise will tend to be the dominant noise, when the laser average power is increasing.

7.1.4. Signal-to-Noise Ratio (SNR)

Once we have characterized the noise level at the input of a receiver, it is possible to analyze the SNR. The SNR is an important parameter because it determines the performance of a receiver. In analog receivers, SNR is the main figure of merit and characterizes the quality of the analog link. Assuming that all of the noise sources described previously are uncorrelated, the signal-noise ratio of the link at the single photo-detector can be expressed by:

$$SNR = \frac{\Re^2 P_R^2}{\sigma_s^2 + \sigma_T^2 + i_{RIND}^2} = \frac{\Re^2 P_R^2}{2q(I_P + I_D)B + \frac{4kTB}{R_L} + RIN \cdot I_D^2 B} \quad (81)$$

From Eq. (81), P_R is the received optical power at the end of the optical link. On the other hand, according to the Figure 9 and Eq. (42), and considering that the modulated optical power at the output of MZ-IM is propagated through an optical fiber of length L, the P_R can be written by $P_R = 10^{-\alpha_{fiber} L / 10} P_{out}$. Here α_{fiber} is the optical fiber loss, and L is the

transmission distance of the optical fiber. In that case if we consider that $\pi V_m/V_\pi \ll 1$ then Eq (81), can be rewritten as

$$SNR = \frac{\mathfrak{R}^2 \left(10^{-\alpha_{fiber} L/10} P_{out} \right)^2}{2q(I_p + I_D)B + \frac{4kTB}{R_L} + RIN \cdot I_D^2 B} = \frac{\mathfrak{R}^2 \left(\left(10^{-\alpha_{fiber} L/10} \right) \frac{\alpha P_{in}}{2} \left\{ \frac{\delta^2}{2} - \delta \left[\frac{\pi V_m}{V_\pi} \right] \right\} \right)^2}{2q(I_p + I_D)B + \frac{4kTB}{R_L} + RIN \cdot I_D^2 B} \quad (82)$$

This equation provides several insights into the SNR behavior of a receiver. Notice that as expected, increasing the optical power P_{in} increases the SNR. On the other hand, increasing the bandwidth of the receiver, B , reduces the SNR. The denominator of Eq. (82) shows the contribution of thermal noise, shot noise and RIN to SNR. An interesting point is that as R_L increases, the effects of thermal noise decrease. In a practical circuit, however, R_L cannot be increased too much because it will reduce the bias headroom of the photo-detector.

7.1.5. Experimental (SNR)

In order to measure the quality of the received signal, it was necessary to experimentally quantify the parameter of signal-to-noise ratio (SNR) for both cases (TV transmitted and recovered in the photonic link).

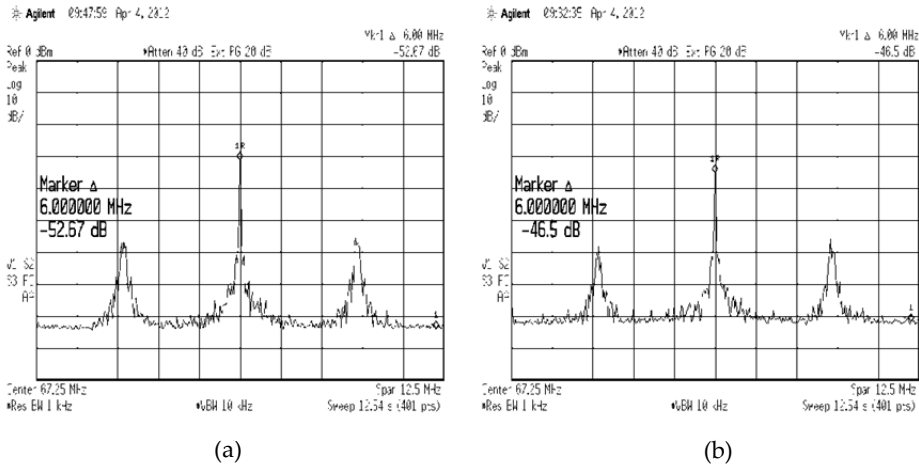


Figure 23. TV signals at 67.25 MHz in order to measure experimentally the SNR parameter, (a) transmitted (b) recovered.

As can be seen from figure 23(a), the SNR measured in a bandwidth of 6 MHz was of 52.67 dB. On the other hand the SNR measured in the receiver was of 46.5 dB as shown in figure 23(b). Notice that the SNR measured in the receiver was degraded by 6.17 dB due to the optical fiber loss and it could be improved substantially with the addition of another stage of electrical amplification at the end of the link. However, values of SNR > 45 dB

ensure a good quality of images [51]. The differential gain and differential phase were not measured in this chapter. Nevertheless we have experimentally demonstrated that the generated microwave signal (relaxation oscillation frequency) by using direct detection can be used as information carriers in a multiplexed transmission system based in an analog photonic link and we have used a TV signal of test to verify it.

8. Conclusions

In this chapter we have described optical components used in the proposed experimental setup, as well as, we have experimentally demonstrated that two DFB lasers biased in the low laser threshold current region showed relaxation oscillation frequencies in the laser intensity. These frequencies were seen as sidebands on both sides of the main laser line when the optical spectrum was analyzed with a spectrum analyzer. This result allowed the generation of microwave signals on C band by using the operation principle of direct detection. Along with the proposed experimental setup in this work, an analog NTSC TV signal was simultaneously transmitted in an analog photonic link by using relaxation oscillation frequency as information carriers located at 4 and 5 GHz. The TV signal was received satisfactorily when the local oscillators were synchronized in the receiver. For our proposed experimental setup to be recovered the transmitted information successfully, it was necessary to have additional amplifiers which adapt the power levels, improving the quality of the signals. The results obtained in this work ensure that as an interesting alternative, several modulation schemes can be used for transmitting not only analog information but also digital information by using relaxation oscillation frequencies as information carriers. The proposed experimental setup described here can generate continually tuned microwaves. In addition, we can use this feature to transmit several TV signals using frequency division multiplexing schemes (FDM) and wavelength division multiplexing (WDM) techniques, not only point to point but also by using bidirectional systems, exploiting the use of mature microwave signal processing techniques, where multiple signals are multiplexed in the microwave domain and transmitted by a single optical carrier when subcarrier multiplexing (SCM) schemes are proposed. To the best of our knowledge, this is the first published work on the employ of relaxation oscillation frequencies as information carriers for transmitting analog TV signals on a long distance photonic link. In addition, as an alternative of analog photonic links, our proposal shows outstanding performance.

Author details

Alejandro García Juárez

University of Sonora, Department of Physics Research, Mexico

Ignacio Enrique Zaldívar Huerta

National Institute of Astrophysics, Optics and Electronics. Department of Electronics, Mexico

Jorge Rodríguez Asomoza

University of the Americas-Puebla, Department of Electronics, Mexico

María del Rocío Gómez Colín
University of Sonora, Department of Physics, Mexico

Acknowledgement

This work was supported by The Mexican Consejo Nacional de Ciencia y Tecnología (CONACyT), (grant No 102046).

9. References

- [1] Kai Wang, Xiaoping Zheng, Hanyi Zhang, and Yili Guo. A Radio-Over-Fiber Downstream Link Employing Carrier-Suppressed Modulation Scheme to Regenerate and Transmit Vector Signals. *IEEE Photonics Technology Letters* 2007; vol. 19, no. 18, pp. 1365-1367.
- [2] D. Novak, A. Nirmalathas, C. Lim, C. Marra, and R. B. Waterhouse. Fiber-radio-challenges and possible solutions. *Topical Meeting Microwave Photonics* 2003, Sep. 10–12, (2003).
- [3] X. Zhang, B. Liu, J. Yao, K. Wu, and R. Kashyap. A novel millimeter-wave-band radio-over-fiber system with dense wavelength-division multiplexing bus architecture. *IEEE Transactions on Microwave Theory and Techniques* 2006; vol. 54, no. 2, pp. 929–937.
- [4] Stavros Iezekiel. *Microwave Photonics Devices and Applications*. John Wiley; 2009.
- [5] Xue Jun Meng. A Dispersion Tolerant Analog Optical Receiver for Directly Modulated RF Photonic Links. *IEEE Photonics Technology Letters* 2007; vol. 19, no. 6, march 15
- [6] Spiros Mikroulis, Sotiris Karabetos, Evaggelos Pikasis, Aristidis Chipouras and Athanase Nassiopoulos. Evaluation on the performance of Distributed Feedback Lasers (DFB) for Radio-Over-Fiber (RoF) Applications. *International Conference on Telecommunications & multimedia, Greece* 2006.
- [7] A. Baylón-Fuentes, P. Hernández-Nava, A.García-Juárez, I. E. Zaldívar-Huerta, J. Rodríguez-Asomoza, G. Aguayo-Rodríguez and R. Gómez-Colín. Modulation of Relaxation Oscillation Frequency of a DFB Laser by Using Direct Detection. *Broadband Access Communications Technologies V, Proc. of SPIE Vol. 7958*, 2011.
- [8] A.J. Seeds. Broadband wireless access using millimetre-wave over fibre systems. *IEEE MTTs Int. Microwave Symp.*1997; vol.1, pp. 23-25.
- [9] W.H. Loh, C.L. Tang. Polarization modulation for optical-microwave applications in phased array antennas. *IEEE Photonics Technology Letters* 1991; vol.3 no. 5 pp. 478-480.
- [10] J.J. O'Reilly, P.M. Lane. Fibre-supported optical generation and delivery of 60 GHz signals. *Electronics Letters* 1994; vol. 30, no. 16, pp. 1329-1330.
- [11] D.C. Scott, D.V. Plant, H.R. Fetterman. 60 GHz sources using optically driven heterojunction bipolar transistors. *Applied Physics Letters* 1992; vol. 61, no. 1, pp. 1-3.
- [12] J.B. Georges, M. -H. Kiang, K. Heppell, M. Sayed, K.Y. Lau. Optical Transmission of Narrow-Band Millimeter Wave Signals by Resonant Modulation of Monolithic Semiconductor Lasers. *IEEE Photonics Technology Letters* 1994; vol. 6 no. 4 pp 568-570.

- [13] C.R. Lima, D. Wake, P.A. Davis. Compact optical millimetre-wave source using a dual-mode semiconductor laser. *Electronics Letters* 1995; vol. 31 no. 5, pp. 364-366.
- [14] L. Goldberg, A.M. Yurek, H.F. Taylor, J.F. Weller. 35 GHz microwave signal generation with an injection-locked laser diode. *Electronics Letters* 1985; vol. 21, no. 18, pp. 814-815.
- [15] P. Shen, N.J. Gomes, P.A. Davis, W.P. Shillue, P.G. Huggard, B.N. Ellison, in: *Proc. Int. Top. Microw. Photon. Meeting*, 2003.
- [16] D. Wake, C.R. Lima, P.A. Davies. Optical generation of millimeter-wave signals for fiber-radio systems using a dual-mode DFB semiconductor laser. *IEEE Transaction on Microwave Theory and Techniques* 1995; vol. 43, no. 9, pp. 2270 – 2276.
- [17] R.T. Ramos, A.J. Seeds. Fast heterodyne optical phase-lock loop using double quantum well laser diodes. *Electronics Letters* 1992; vol. 28 no. 1, pp 82-83.
- [18] A. García-Juárez, I. E. Zaldívar-Huerta, G. Aguayo-Rodríguez, J. Rodríguez-Asomoza, R. Gómez-Colín, A. Vera-Marquina, M. C. Acosta-Enriquez, A. Rojas-Hernández. Optical heterodyne technique for generating and distributing microwave signals. *Broadband Access Communications Technologies IV, Proc. of SPIE Vol. 7620*, 2010.
- [19] A. García-Juárez, I. E. Zaldívar-Huerta, G. Aguayo-Rodríguez, J. Rodríguez-Asomoza, R. Gómez-Colín, A. Rojas-Hernández. Coherent demodulation of microwave signals by using optical heterodyne technique with applications to point to point indoor wireless communications systems. 2011 *J. Phys.: Conf. Ser.* 274 012008, doi:10.1088/1742-6596/274/1/012008. (<http://iopscience.iop.org/1742-6596/274/1/012008>)
- [20] Jianping Yao. *Microwave Photonics. Journal of Lightwave Technology* 2009; vol. 27, no. 3, pp. 314-335.
- [21] L. Goldberg, H. F. Taylor, J. F. Weller, and D. M. Bloom. Microwave signal generation with injection locked laser diodes. *Electron. Letters* 1983; vol. 19, no. 13, pp. 491-493.
- [22] U. Gliese, T. N. Nielsen, M. Bruun, E. L. Christensen, K. E. Stubkjaer, S. Lindgren, and B. Broberg. A wideband heterodyne optical phaselocked loop for generation of 3–18 GHz microwave carriers. *IEEE Photon. Technol. Letters* 1992; vol. 4, no. 8, pp. 936–938.
- [23] A. C. Bordonalli, C. Walton, and A. J. Seeds. High-Performance phase locking of wide linewidth semiconductor lasers by combined use of optical injection locking and optical phase-lock loop. *J. Lightwave Technology* 1999; vol. 17, no. 2, pp. 328–342.
- [24] Z. F. Fan and M. Dagenais. Optical generation of a mHz-linewidth microwave signal using semiconductor lasers and a discriminator-aided phase-locked loop. *IEEE Trans. Microw. Theory Tech.*, 1997; vol. 45, no. 8, pp. 1296–1300.
- [25] J. J. O'Reilly, P. M. Lane, R. Heidemann, and R. Hofstetter. Optical generation of very narrow linewidth millimeter wave signals. *Electron. Letters* 1992; vol. 28, no. 25, pp. 2309–2311.
- [26] J. J. O'Reilly and P. M. Lane. Remote delivery of video services using mm-wave and optics. *J. Lightw. Technol.* 1994; vol. 12, no. 2, pp. 369–375.
- [27] P. Shen, N. J. Gomes, P. A. Davies, W. P. Shillue, P. G. Huggard, and B. N. Ellison. High-purity millimeter-wave photonic local oscillator generation and delivery. in *Proc. Int. Microw. Photonics Topical Meeting*, Sep. 10–12, 2003, pp. 189–192.

- [28] G. Qi, J. P. Yao, J. Seregelyi, C. Bélisle, and S. Paquet. Generation and distribution of a wide-band continuously tunable mm-wave signal with an optical external modulation technique. *IEEE Trans. Microw. Theory Tech.* 2005; vol. 53, no. 10, pp. 3090–3097.
- [29] X. Chen, Z. Deng, and J. P. Yao. Photonic generation of microwave signal using a dual-wavelength single-longitudinal-mode fiber ring laser. *IEEE Trans. Microw. Theory Tech.* 2006; vol. 54, no. 2, pp. 804–809.
- [30] X. Chen, J. P. Yao, and Z. Deng. Ultranarrow dual-transmission-band fiber Bragg grating filter and its application in a dual-wavelength single-longitudinal-mode fiber ring laser. *Opt. Lett.* 2005; vol. 30, no. 16, pp. 2068–2070.
- [31] H. Zandi, M. Bavafa, M. Chamanzar, and S. Khorasani. Analysis of power harmonic content and relaxation resonant frequency of a diode laser. *Proc. SPIE*, Vol. 6468, No. 64680J, 2007.
- [32] H. Zandi, M. Bavafa, M.R. Chamanzar and S. Khorasani. Harmonic Content and Relaxation Resonant Frequency of a Modulated Laser Diode. *Transactions D: Computer Science & Engineering and Electrical Engineering* 2009; Vol. 16, No. 2, pp. 145-156.
- [33] M. Bavafa, H. Zandi, M. Chamanzar, and S. Khorasani. Optimal Operation Point for the Primary Harmonic Content of a Modulated Laser Diode. *Proceedings of the 6th WSEAS International Conference on Microelectronics, Nanoelectronics, Optoelectronics, Istanbul, Turkey, May 27-29, 2007.*
- [34] L.A. Coldren, and S.W Corzine. *Diode Lasers and Photonic Integrated Circuits.* John Wiley & Sons; 1995.
- [35] B. E. A. Saleh. *Fundamentals of Photonics.* John Wiley & Sons, Inc; 1991. pp. 624-626.
- [36] A. Baylón-Fuentes, P. Hernández-Nava, A.García-Juárez, I. E. Zaldívar-Huerta, J. Rodríguez-Asomoza, G. Aguayo-Rodríguez and R. Gómez-Colín. Modulation of Relaxation Oscillation Frequency of a DFB Laser by Using Direct Detection. *Broadband Access Communications Technologies V, Proc. of SPIE Vol. 7958*, 2011.
- [37] A.García-Juárez, I. E. Zaldívar-Huerta, J. Rodríguez-Asomoza³, R. Gómez-Colín, A.G Rojas-Hernández, D. Berman-Mendoza, R. Gómez-Fuentes and A. Vera Marquina. Analog Photonic Link by Using DFB lasers Operated in the Low Laser Threshold Current Region and External Modulation. *Broadband Access Communications Technologies VI, Proc. of SPIE Vol. 8282*, 2012.
- [38] D. Derickson. *Fiber Optic Test and Measurement.* Prentice Hall PTR; 1998. pp. 175-179.
- [39] C. H. Cox. *Analog Optical Links: Theory and Practice.* Cambridge: Cambridge University Press; 2004, pp. 37–38.
- [40] X. Jun Meng, A. Karim. *Microwave Photonic Link with Carrier Suppression for Increased Dynamic Range.* *Fiber and Integrated Optics*, Taylor & Francis Group; 2006. pp. 161- 174.
- [41] P. S. Henry. Lightwave primer," *IEEE J. Quantum Electron.* 1985; vol. QE-21, pp. 1862–1879.
- [42] Jha, A.R. State of the Art Fiber Optic Components and Photonic Devices for Optical Communication and High Speed Transmission. *31st European Microwave Conference*, 2001.
- [43] B. E. A. Saleh. *Fundamentals of Photonics.* John Wiley & Sons, Inc; 1991. pp. 193-237

- [44] Donald K. Wilson. Polarization control aids fiber component testing. *Lasers Focus World* 1997; pp. 129–133.
- [45] José Capmany, F. Javier Fraile-Peláez y Javier Martí. *Dispositivos de Comunicaciones Ópticas*. Editorial Síntesis.
- [46] R. A. Bergh, G. Kotler y H. J Shaw. *Electron. Lett.* , 1980; p 260.
- [47] S. K. Sheem y T. Giallorentzi. *Opt. Lett.* 1979; p 29.
- [48] E. Garmire. Sources, modulation, and detectors for fiber-optic communication systems, in *Fiber Optics, Handbook*. Edited by M. Bass, McGraw-Hill, New York; 2002 pp. 4.1–4.78,
- [49] Leonid Kazovsky, Sergio Benedetto and Alan Willner. *Optical Communications Systems*, Artech House; 1996.
- [50] Abhay Joshi, Xinde Wang, Dan Mohr, Don Becker, and Christoph Wree. Balanced photoreceivers for analog and digital fiber optic communications. *Proc. of SPIE Vol.* 5814, 2005.
- [51] M. Kowalczyk and J. Siuzdak. Multi-channel am video transmission beyond the baseband of multimode fiber. *Microwave and optical technology letters* 2010; vol. 52, no. 2, pp. 435-438.